Electrochemical study on the reduction of Si and Ti from molten $TiO_2 - SiO_2 - Al_2O_3 - MgO - CaO$ slag

Samuel Martin-Treceno[1], Thomas Hughes[1], Nicholas Weaver[1], Aaron T. Marshall[1], Matthew J. Watson[1,2] and Catherine M. Bishop[3,z]

[1] Department of Chemical and Process Engineering, University of Canterbury, Private Bag 4800, Christchurch, 8140 New Zealand

[2] Biomolecular Interaction Centre, University of Canterbury, Christchurch, New Zealand

[3] Department of Mechanical Engineering, University of Canterbury, Private Bag 4800, Christchurch, 8140 New Zealand

[z] Corresponding Author Email Address: catherine.bishop@canterbury.ac.nz

Accepted 3 May 2021

Abstract. The reduction process during the electrochemical production of titanium via the electrolysis of molten $TiO_2 - SiO_2 - Al_2O_3 - MgO - CaO$ slags has been investigated. A laboratory scale, electrolytic cell was designed to study the effect of TiO_2 concentration at ultra-high temperatures. Galvanostatic and potentiostatic experiments were performed and results were consistent with thermodynamic predictions using FactSage. We demonstrate the direct production of Si-Ti alloys from the molten oxide mixture. The reduction of Si and Ti ions from the melt on a molybdenum electrode is a complex process that combines electron transfer and chemical phenomena. For the concentrations studied, the extraction of pure metallic Ti directly from ironmaking slag is unlikely without the prior removal of SiO_2 or other chemical modifications to the system.

Keywords: ultra-high-temperature electrochemistry, molten oxide electrolysis, Ti-Si alloys, metal extraction, titanium-bearing slags

Submitted to: *Journal of Electrochemical Society*

1. Introduction

Focus on the circular economy is pushing research to find beneficiation techniques for abundant industrial by-products [1]. Ironmaking slag is the biggest by-product of the steel industry, and hence researchers have been attracted to study ways to extract further value [2]. Extracting high purity metals is a high added-value solution, which would allow traditional recycling practices to still be used for the remaining slag material [3], potentially increasing its value [4]. Furthermore, the direct electrolysis of molten slag has the potential to cut the direct emissions of green house gases associated with traditional metallurgical practices [5, 6].

Study of the ionic nature of slags has been gaining relevance since the beginning of the 20th century [7]. These metal oxide mixtures have proved to be good high temperature solvents of 3d transition metal oxides, achieving metal ion concentration higher than industrial electrolytes [8]. Moreover, the presence of silica in the oxide network provides the thermal stability needed to operate at the high temperatures required to cast a liquid metallic product. Due to the timely need to find more sustainable alternatives to the current steelmaking practices [9], the use of ironmaking slag as a secondary source of metal has been mostly linked to the production of iron [5, 10]. The production of iron from the electrolysis of molten slag benefits from the fast kinetics of high temperature operation and potentially high selectivity as iron oxide has the lowest thermodynamic stability compared to the other slag constituents.

At standard conditions, the Gibbs energy required for the reaction of a pure molten oxide into the most stable metallic phase can be obtained from the Ellingham Diagram. At temperatures in the vicinity of its liquidus temperature [11], $TiO_2 - SiO_2 - Al_2O_3 - MgO - CaO$ slags are chemically stable and no reduction reactions are predicted to occur spontaneously for any pure constitutive oxide. Upon the application of a potential, any iron oxide will be reduced first as it requires the minimum thermodynamic cell voltage [12]. Silica is the component of the slag that will be next to reduce, closely followed by titania. Thermodynamics seems to indicate that an electrolytic route for the production of more reactive 3d metals, such as titanium, might need silica-free electrolytes [8].

However, in this study the electrolyte is not a pure molten oxide but a solution of five different oxides. The non-ideal properties of the molten slag system will shift the decomposition voltages predicted [13]. The small electrochemical window of operation between the decomposition of silica and titania [11], along with the high concentration ($> 20\,\mathrm{wt}\%$) of titania commonly present in ironmaking slags [14] have attracted research attention [15, 16]. Recently, we electrochemically produced Ti-Si alloys from molten $TiO_2 - SiO_2 - Al_2O_3 - MgO - CaO$ slag [11]. Our proof of concept study showed that reduction of Ti and Si was possible, but it did not elucidate the thermodynamic

conditions for the reduction.

In this work, galvanostatic and potentiostatic electrolysis experiments were performed to study the electrochemical reduction process of titanium and silicon ions from molten $TiO_2 - SiO_2 - Al_2O_3 - MgO - CaO$ slags at 1823 K. The temperature was selected because it is the temperature at which slag is tapped from the local ironmaking process, but it is below the melting point of Ti so that a solid product is anticipated. Thermodynamic predictions using FactSage [17] were used to investigate the effect of composition changes on the cell voltages required to deposit silicon and titanium from the slag. Characterisation of the products of the molten oxide electrolysis (MOE) experiments provided insight into the kinetic processes. The Ti-Si alloy produced in these experiments are gaining traction in the market for their high temperature structural properties [18, 19].

2. Experimental

2.1. Sample preparation

Two $TiO_2 - SiO_2 - Al_2O_3 - MgO - CaO$ samples, Slag A and Slag B, were prepared by calcining reagent grade powder starting materials. The final compositions of the samples were measured by x-ray fluorescence spectroscopy (XRF, Siemens/Bruker SRS3000), and are reported in Table 1. Sample production has been described previously for these mixtures [11].

2.2. Experimental set-up

For this study, a vertical tube furnace (GSL-1700x-100VT-UL, MTI Corp.) was used to achieve the temperatures required to melt the slags and perform electrochemical measurements.

2.2.1. Vertical tube furnace An alumina tube ($Al_2O_3 > 99.5\,\%$, 90.2 mm ID x 101.7 mm OD x 1000 mm H, MTI Corp.) was used to contain the entire system inside the vertical tube furnace, and a graphite crucible (45 mm OD x 35 mm ID x 80 mm H, Baofeng Graphite) was used to contain the sample. A secondary graphite crucible (80 mm OD x 60 mm ID x 60 mm H, Graphite Store) was used to prevent any damage in case of leakage. The samples were placed in the centre of the hot zone using an internal support structure made of molybdenum (Figure 1A).

The design allowed electrodes to be raised/lowered into the molten material while maintaining an inert environment inside the tube. In order to reach the ultra-high temperature required for operation, insulating alumina blocks (Al_2O_3 foam, 80 mm D x 65 mm H, MTI Corp.) were placed on either side of the furnace hot zone. The two flanges (304 SS, MTI Corp.) sealing the alumina tube were water-cooled during operation to

prevent them from overheating due to radiative heat transfer. A type B thermocouple (National Basic Sensor) was used to monitor the temperature in the secondary crucible.

To begin the experiments, while the furnace was at room temperature, the system was purged with zero grade Ar (99.999 %, BOC) for 90 min at a flow rate of 500 $cm^3\,min^{-1}$. Once the oxygen content, detected by an oxygen analyser (Thermox CG-1000), was confirmed to be below 100 ppm, the flow rate was lowered to 150 $cm^3\,min^{-1}$ for the remainder of the experiment. After the purge sequence, the sample was heated at a rate of 1 $K\,min^{-1}$ to an internal temperature of 1823 K. Once the system had been at temperature for an hour, the electrodes were lowered into the slag. During that process, the resistance between the working and counter electrode was measured with a voltmeter (Fluke 117 Handheld Digital Multimeter). A drop in the resistance value indicated when the electrodes had contacted the slag. The electrodes were then lowered to their desired depth, estimated to be (15 ± 5) mm. The experiment finished by cooling the system at 1 $K\,min^{-1}$ down to room temperature.

Upon cooling, the working electrode (WE) was cross-sectioned perpendicular to the electrode's longitudinal axis, using a high-speed diamond saw (Bühler). The sample was set in a conducting mounting compound (ProbeMet), and polished using progressively finer grades of silicon carbide paper (180, 320, 400, and 600 grit) and 9 µm diamond suspension. The composition and microstructure of the electrolysis product was examined using a scanning electron microscope (SEM, JEOL JSM-IT300LV) with LaB6 filament equipped with a X-Maxä 50 silicon drift energy dispersive spectroscopy (EDS) detector.

The phases present in solidified bulk slag from control experiments were identified using x-ray diffraction (XRD) analysis. Fine crushed powder samples were scanned using a Bruker D8 instrument with Co K-α radiation. The 2θ range was 30-110 degrees.

2.2.2. Electrochemical measurements A three-electrode configuration was used with the graphite crucible as the counter electrode, and two molybdenum wires (Mo > 99.95 %, 600 mm L, Extreme Bolt & Fasteners) serving as the working and pseudo-reference electrodes. Molybdenum was used as the working and pseudo-reference electrode material as its physical properties make it robust enough for a wire to be inserted repeatedly into the molten slag. Molybdenum is an affordable, easily machinable and high melting temperature (2896 K) metal. However, molybdenum is not a suitable counter electrode material since it reacts easily with oxygen at the temperatures of interest, forming volatile oxides [20].

Galvanostatic and potentiostatic electrolysis experiments were performed using power supplies (Keithley 2260B-30-72 and Powertech MP3090, respectively). The voltages between the electrodes were recorded with a data logger (Measurement Computing 1808). The pseudo-reference electrode (1 mm D) was sheathed in an alumina

($Al_2O_3 > 99.8\,\%$, 6.35 mm OD, 1.3 mm ID, McDanel Advanced Ceramics) single bore tube. The top of the tube bore was sealed to prevent oxygen from entering the system. A thicker molybdenum rod (6 mm D, 600 mm L) was used as the working electrode in order to minimize the voltage drop along its length. However, to avoid large currents that the equipment could not support, the electrode's active area in contact with the slag was minimized by decreasing down to 2 mm the diameter of a 20 mm section at the end of the rod (Figure 1B).

2.3. Computational thermodynamic calculations

Thermodynamic cell voltages for the electrolytic extraction of metals from $TiO_2 - SiO_2 - Al_2O_3 - MgO - CaO$ slags were predicted with the thermodynamic software FactSage 7.2 [17], using model parameters from its FToxid and FactPS databases. Thus, thermodynamic activities, based on validated solution models and free energies of intermetallic products rather than unit activities, as in Ellingham diagrams, or first-order ideal solution approximations, were used. The cell voltages were calculated from the Nernst equation:

$$E_{cell} = E^{\circ}_{cell} - \frac{RT}{nF} \cdot \ln \frac{\prod a^{\nu}_{products}}{\prod a^{\nu}_{reactants}} \tag{1}$$

where E°_{cell} is the thermodynamic (minimum) cell voltage at standard conditions, R is the universal gas constant, T is the temperature of interest, ν are the stoichiometric coefficients and a_i are the activities of the species present in the reaction. All reactions were based on the formation of one mole of O_2 as the anodic reaction:

$$2O^{2-} \rightarrow O_2 + 4e^- \tag{2}$$

while the cathodic reaction was the reduction of one or two of the metal oxides from the slag. This allows direct comparison of the minimum energy required to drive the various reduction reactions. The energy required will vary if CO_2 evolution is assumed to be the anodic reaction, and the reduction potentials would need to be calculated against this half-cell reaction instead.

The conditions inside the vertical tube furnace were simulated to model the gas phase. As a graphite crucible and an Ar purge gas were used in the experiments, the gas phase was modelled using 15 g of Ar, the approximate amount contained in the vertical tube furnace at standard pressure and temperature, and the oxygen activity in the gas was determined from the equilibrium with graphite. Consequently, O_2 activities were around 10^{-17} at the temperatures investigated. The activity of unary metallic products was assumed to be one. Cell voltages where the metallic reduction product was an intermetallic formed by co-reduction of two metals or by reaction of a reduced metal from the slag with the electrode material were also predicted. In those cases, the activity of the compound was assumed to be one and the standard chemical potential was the molar free energy of formation extracted from FactSage.

3. Results and Discussion

3.1. Materials compatibility

In order to guarantee that they are going to be able to perform as originally designed, ideally, all components should be inert at the conditions they are going to be exposed to. Graphite (crucible and counter electrode) and molybdenum (electrode and cell's support structure) are the main materials used in the electrochemical cell. An accurate knowledge of their behaviour in the presence of oxygen is of vital importance. Many metals upon contact with oxygen form an adherent protective oxide film at their surface which prevents further oxidation until a certain temperature is reached [21]. Gulbrasnsen *et al.* [20] established that for molybdenum this temperature is 873 K. Additionally, they observed that between 873 K and 1073 K both oxide film formation and oxide volatility occur, while above that molybdenum trioxide is spontaneously formed. The concentration of oxygen inside the vertical tube furnace was not measured for these experiments, but the negligible weight change of the molybdenum support rods and the graphite crucible after each experiment confirmed the air-tightness of the designed system.

Thermodynamic calculations predicted no spontaneous metallothermic reaction of molybdenum with any of the components of the molten slag. Because molybdenum is susceptible to oxidation by iron oxide slags [22], the stability of the molybdenum as an electrode materials at the operating conditions was experimentally verified. Post-mortem electron microscopy of control experiments, *i.e.*, experiments in which the system underwent the same thermal treatment but without electrolysis, validated this prediction.

Additionally, no evidence of carbide formation was detected from post-mortem EDS analyses in the slag when fired using a graphite crucible, and no sign of any graphite was detected in any XRD pattern. This is consistent with the non-reactive wetting behaviour observed in the present experiments (Figure 2), and with observations by Van der Colf and Howat [23], who studied ironmaking slags in graphite crucibles.

3.2. Initial electrolysis experiments

In electrolytic cells, a cell voltage threshold, E°_{cell}, has to be exceeded for ionic charge transfer to occur during an electrochemical reaction at the electrodes. The corresponding thermodynamic cell voltages for the reduction of metallic cations in the slag were predicted as a function of temperature for Slag A chemistry (Figure 3). Titanium, the only transition metal in the slag, can exist in multiple oxidation states, reported to be Ti^{4+}, Ti^{3+} and Ti^{2+} in Ti-bearing slags, with a distribution that depends on slag composition, temperature and oxygen partial pressure. Tranell *et al.* [24] reported only Ti^{3+} and Ti^{4+} oxidation states at temperatures and oxygen partial pressures similar to ours in $CaO - SiO_2 - TiO_x$ slags with 7.2 wt% – 52.3 wt% TiO_2, where the Ti^{3+}: Ti^{4+}

ratio was less than one and followed the ideal proportionality with the partial pressure of oxygen. Therefore, Ti^{3+} is included in our thermodynamic predictions along with Ti^{4+}. The predicted thermodynamic threshold for the decomposition reactions in the electrolyte indicated that first silicon, and then titanium ions will be reduced from the melt, with a potential window less than 200 mV between the two.

This prediction was checked against experimental potentiostatic experiments performed on Slag A. For 150 min, a constant cell voltage of -2.0 V was applied at an internal temperature of 1823 K inside the vertical tube furnace. During this time the average current was 4 A, and 130 g of slag were electrolyzed until the system started its cooling sequence. The current density was estimated to be $(4.1 \pm 1.5)\,\mathrm{A\,cm^{-2}}$, where the uncertainty is half the difference between the upper and lower estimates originating from the minimum and maximum electrode immersion depths. At this point the applied voltage was halted and the working electrode was raised from the melt to allow easier sample manipulation for post-mortem microscopy analysis. The backscattered-electron images of the polished material indicated that phase segregation occurred on cooling (Figure 4). Large blocky spinel crystals and dendritic perovskite crystals were the main crystalline phases that precipitated from the slag below its liquidus temperature. In our previous study [11], in-situ XRD analysis identified this spinel phase as the first stable solid phase to form in the slag below the liquidus. The phase identification on cooling is consistent with that reported by Ratchev and Belton [25] in similar titanomagnetite smelting type slags. Similarly, they also observed crystals in the slag segregating to the bottom of the container.

A ring of electrolytically reduced material surrounding the molybdenum working electrode is noticeable in Figure 4C. The composition of this deposit adjacent to the cathode was investigated by EDS, where five different regions were identified (Figure 5). Region I is the core of the molybdenum working electrode. Regions II and IV contain products of the electrolysis. Regions III and V contain phases from the region of the bulk electrolyte that has been depleted of Si and Ti.

Region II is bonded to the surface of the working electrode where a combination of Si-Ti-Mo phases were formed. Since the cell voltage during the potentiostatic experiment was held above the thermodynamic threshold at which titanium and silicon ions can be reduced from the slag (see Figure 3), it is speculated that the product formed is a consequence of a surface alloy reaction that followed the electrochemical reduction of silicon and titanium ions from the melt. According to thermodynamic predictions, the spontaneous formation of Mo_3Si, $MoSi_2$, Mo_5Si_3, TiSi, Ti_5Si_3 and Ti_5Si_4 intermetallic phases is possible at 1823 K (see Table 2). The gradient of metallic alloy compositions formed on the surface of the working electrode is likely the result of different diffusivities of the reduced Si and Ti metals and Mo from the working electrode. The final size distribution of these alloys is expected to be defined by the nucleation kinetics at

the electrode surface, in particular the interfacial free energy barrier and the strain effects [26].

Region IV shares the same features of Region II, including the gradually decreasing concentration of Mo with distance from the working electrode. We speculate that Regions II and IV formed part of a compact reduced layer that grew radially outward from the working electrode with time during electrolysis and that the layer broke on cooling as the electrode was pulled out of the melt. Region III is part of the bulk electrolyte, where crystalline phases have formed during cooling. This agrees with the spinel crystal composition previously identified in the slag, where Ti has partially substituted Al. This also agrees with the formation of a solid solution spinel of magnesium meta-aluminate, $MgAl_2O_4$, and magnesium meta-titanate, $MgTi_2O_4$, observed by Ratchev and Belton [25] for titanomagnetite smelting slags with a similar TiO_2 concentration. Region V is also part of the bulk electrolyte, corresponding to the amorphous slag phase, that is depleted of TiO_2. Due to the presence of TiO_2 in the spinel and perovskite phases, the reduced amount of TiO_2 in the slag cannot be exclusively correlated to the electrolytically produced titanium metal.

In addition to this cathodic ring deposit, areas of bright contrast in the backscatter images were found dispersed in a ring of approximately 1 mm adjacent to the working electrode (Figure 4C). The composition of the speckled phase was determined by EDS analysis to be around $Ti_{1.7}Si$, which is close to the stoichiometric phase Ti_5Si_3 [27]. The difference might be associated to the use of standard-less EDS. The dispersion of this phase through Region V in the slag, instead of being immediately adjacent to the working electrode, was not expected. An explanation for this phenomena is that the Ti_5Si_3 phase is part of a three-dimensional dendritic sponge structure that grew radially outwards from the working electrode and was in electrical contact with it. Any connectivity may be obscured in this two-dimensional cross section. Once the phase had nucleated, dendritic growth would be easy and would minimize the effect of depletion layers in the electrolyte.

Other explanations were evaluated and dismissed. If the intermetallic nucleates in the slag and is not connected to the electrode, then the Si and Ti metals must be electrochemically reduced at the electrode or metallothermically reduced from the oxides in the slag. While Ti_5Si_3 can form spontaneously at 1823 K from Si and Ti with unit activity, $\Delta G^0_{Ti_5Si_3} < 0$, Table 2, the free energy of formation depends on the activities of the metallic reactants in solution, a_{Ti} and a_{Si},

$$\Delta G_{Ti_5Si_3} = \Delta G^0_{Ti_5Si_3} + RT \ln \frac{1}{a^5_{Ti} a^3_{Si}} \tag{3}$$

Consider, electrochemically reduced Si and electrochemically reduced Ti dissolved in the slag phase as the reactants. The solubility of metals in slag should be very small, implying low activities, which will reduce the driving force for formation of the

intermetallic phase $\Delta G_{\mathrm{Ti_5Si_3}}$. Further, the nucleation barrier to intermetallic formation is likely to be significant.

In the Hunter process, dissolved sodium metal in molten sodium chloride enhances that electrolyte's conductivity and allows the reaction to take place in the bulk, where reduced titanium particles nucleate [28]. Lei *et al.* [29] reported that, contrary to the Ellingham diagram, TiO_2 in a Ti-bearing blast furnace slag could be reduced by Si. If electrochemically reduced Si were dissolved in the slag, the concentration and activity are likely small and the free energy of metallothermic reduction reaction $\mathrm{Si}(slag)+\mathrm{TiO_2}(slag) \rightarrow \mathrm{Ti}+\mathrm{SiO_2}(slag)$, $\Delta G = \Delta G_{electrochem} + RT \ln \frac{1}{a_{Si}}$, would be even more positive than the value calculated from the electrochemical step, $\Delta G_{electrochem} = -4F(E_{cell}^{Ti^{4+}} - E_{cell}^{Si^{4+}})$, Figure 3.

If electrochemically reduced Si formed a liquid phase rather than dissolving in the slag, it could be convectively mixed with the slag phase. This free Si cannot spontaneously reduce TiO_2 dissolved in the slag because $\Delta G_{electrochem} > 0$. The free energy for the direct formation of the intermetallic $3\mathrm{Si}(l) + 5\mathrm{TiO_2}(slag) \rightarrow \mathrm{Ti_5Si_3} + 5\mathrm{O_2}(g)$ at 1823 K is also positive, and so this reaction cannot be spontaneous either.

Regardless of its location, the Ti_5Si_3 phase is further evidence of the product of an electrochemical reaction as it was not observed in control experiments with the same thermal treatment but no electrolysis.

3.3. Effect of varying the slag composition on the electrochemical reduction sequence

The initial electrolysis experiment showed that titanium and silicon were deposited together, with titanium seemingly kinetically favoured. This is relevant since with the small potential window between silicon and titanium reduction, kinetics might be able to alter the reduction sequence, and enable selective reduction of titanium. The effect of varying the slag composition and temperature on the electrochemical reduction sequence was predicted using FactSage (Figure 6).

The thermodynamic activities and cell voltages for the constituents of the slag phase were investigated at 1773 K and 1873 K, the range of operating temperatures of ironmaking melters. By varying the ratio of SiO_2 and TiO_2 while keeping the total concentration of the two components in the melt constant, the effect of concurrently extracting silicon along with titanium from the slag on the thermodynamic cell voltages was investigated. For the range of temperatures and compositions studied, the results from the computational model illustrate that the reduction of silicon ions from the melt is always the most favourable. According to the thermodynamic predictions, the change in temperature has a minor effect. The activity of SiO_2 was always greater than that of TiO_2 in the slag, which results in lower cell voltages for the reduction of silicon independent of the amount of TiO_2 in the slag. Titanium reduction is preferred only when there is no silica in the system.

However, the model is purely thermodynamic and has no consideration for the kinetics of the process. Hence, further electrochemical experiments must be performed in order to elucidate the effect of the overpotentials at the electrodes on the reduction sequence. To investigate the kinetics of the reduction, galvanostatic electrolysis was performed on Slag B (with 9 wt% TiO_2 compared to 33 wt% for Slag A). In the experiment, a thinner Mo WE (1 mm D) was used, along with a smaller graphite crucible (20 mm OD x 14 mm ID x 20 mm H, Baofeng Graphite) to contain the 5 g of sample. The current was fixed at 5 A for 317 min at 1823 K inside the vertical tube furnace. The current density was estimated to be $(10.0 \pm 3.8)\,\mathrm{A\,cm^{-2}}$, where the uncertainty is half the difference between the upper and lower estimates originating from the minimum and maximum electrode immersion depths. The resulting cell voltage stabilized over time around -2.4 V, as shown in Figure 7.

For this experiment, the working electrode was not removed from the molten slag after electrolysis, but instead it was allowed to cool in the melt. The rest of the post-mortem microscopy procedure was as previously described, and the composition surrounding the working electrode was mapped using EDS (Figure 8). At -2.4 V, a similar voltage to the potentiostatic electrolysis experiment, the EDS maps show that Ti and Si ions were also reduced from the melt. In accordance with a longer electrolysis time, there is a larger layer of reduced metal on the surface of the molybdenum working electrode compared to the potentiostatic electrolysis of Slag A. Even though the cell voltage exceeded the predicted thermodynamic reduction potentials for Mg^{2+} and Al^{3+}, no clear Mg or Al reduction products were found. Reduced Mg would be in the vapour phase and might be lost to the furnace atmosphere. Reduced Al would be in the liquid phase and should react with the other metals, but no metallic Al was detected at the cathode. A larger cell voltage may be required to overcome the Mg^{2+} and Al^{3+} reduction overpotentials. The various product regions formed in the reduced layer were measured by EDS to experimentally verify the predicted negligible effect of TiO_2 concentration on altering the slag's electrodeposition sequence (Figure 9).

Similar to Slag A, a gradient of alloy composition was formed at the surface of the molybdenum electrode with the reduced Ti and Si metals (Region II), which corresponds to the different Z-contrast in the back-scatter electron image. Si diffused further into the Mo working electrode, lowering its activity towards the thermodynamically stable Mo_5Si_3 alloy. Closer to the interface with the bulk electrolyte (*i.e.*, Region V, also depleted of TiO_2), the concentration of Ti increases in the alloy, forming a gradient of alloy compositions that resembles Region IV in Figure 5. Overall, there is less Ti in the near-cathode reduced metallic region of the titania-lean Slag B compared to the titania-rich Slag A composition, which could be attributed to mass transport limitations. The lack of an intermediate Region III in Figure 9 confirmed that a compact reduced metallic layer likely formed during the potentiostatic electrolysis on Slag A and broke on cooling

due to the effect of pulling the electrode out of the melt.

Alloys of silicon and titanium were also found dispersed in the area of the bulk electrolyte adjacent to the working electrode in Slag B. Hence, in this work, Ti was not selectively extracted as the electrolysis product for any of the TiO_2-bearing silicate slags studied here. Estimates of the current efficiency for Ti and Si co-reduction yielded (1.4 ± 0.4) % for Slag A and (0.16 ± 0.05) % for Slag B. These rough estimates assumed the volume fraction of dispersed intermetallic was equal to the area fraction from image analysis, all reduced Ti and Si formed Ti_5Si_3 product and 40 mol of electrons were consumed per formula unit. The uncertainty is half the difference between the upper and lower estimates originating from the minimum and maximum electrode immersion depths. These low efficiencies clearly show that significant current was not used for Ti^{4+} or Si^{4+} reduction, and the most likely explanation is losses due to electronic, as opposed to ionic, conductivity of the electrolyte. The experiments were conducted in a strong reducing atmosphere due to the graphite crucible, and the slag turned black after both electrochemical and control experiments, suggesting a high concentration of Ti^{3+} consistent with high electronic contributions to electrical conductivity [30]. This explanation is validated by experiments on related $TiO_2 - SiO_2 - Al_2O_3 - MgO - CaO$ slags in a floating zone furnace in argon with $p_{O_2} = 10^{-6}$: a current efficiency of (29 ± 6) % for electrolysis of a slag with 21 wt% TiO_2 at 1903 K was achieved considering just reduction of Ti^{4+} [11], and the fraction of total current borne by electronic carriers was determined to be 0.24 at 1823 K in a slag with 33 wt% TiO_2 [12].

The results indicate that the extraction of pure metallic Ti from $TiO_2 - SiO_2 - Al_2O_3 - MgO - CaO$ slag is unlikely without the prior removal of SiO_2. Even though it was out of the scope of the current study, the small potential window between the reduction of silicon and titanium ions from the melt motivates the further study of the effect of chemical modifications to the oxide system, such as changes in the concentration of the electronegative species [31], on the deposition series of the electrolyte.

While producing titanium metal would be the highest added-value product, the proven electrolytic extraction of Ti-Si alloys could still be a profitable endeavour as these alloys are gaining traction in the market for their use as high-temperature structural materials [19]. Ti-Si intermetallics have a wide range of potential applications [32], from microelectronics to the aerospace industry, due to their low density ($4.32\,\mathrm{g\,cm^{-3}}$ [18]), high melting point (up to 2403 K for Ti_5Si_3 [27]), and high temperature stiffness (from room temperature to 1273 K, the Young's modulus only decreases from 160 GPa to 143 GPa for Ti_5Si_3, and from 250 GPa to 215 GPa for $TiSi_2$ [33]). Traditionally, these alloys have been produced from pure Si and Ti metals which are reacted to form intermetallics and solid solutions of the two elements [18]. Considering the price of metallic Ti and the extra processing required to form Ti-Si alloys, electrolysis from a molten slag has the potential to reduce the costs of production. A further, in-depth techno-economical study is required to assess the viability of this production method.

4. Conclusions

This work demonstrates the production of high purity alloys as an avenue to reuse TiO_2-rich ironmaking slag, an industrial by-product. Experiments indicate that titanium-silicon alloys are the main products of the electrochemical reduction of $TiO_2 - SiO_2 - Al_2O_3 - MgO - CaO$ slags. Results were consistent with thermodynamic predictions using FactSage, where the thermodynamic window between Si and Ti reduction was predicted to be less than 0.2 V at slag process temperatures 1773 K to 1873 K. Changing the amount of TiO_2 and SiO_2 in the system did not yield either titanium or silicon as a pure metallic product. To alter the electrochemical sequence, future work could explore modifying the chemistry of the system, *e.g.*, using a supporting electrolyte.

Acknowledgments

The authors wish to acknowledge contributions from Dr. Ian Brown and Dr. Yaodong Yia in the sample preparation, and from Leigh Richardson, Frank Weerts, Stephen Buezenburg, Graham Furniss, and Stephen Hood who offered their technical expertise, and produced the various parts of the experimental rig. This research was funded by NZ Ministry of Business, Innovation and Employment (MBIE) under the contract CONT-46287-CRFSI-UOC.

References

[1] United Nations. The sustainable development goals report. Technical report, United Nations, 2019.

[2] Teresa Annunziata Branca, Valentina Colla, David Algermissen, Hanna Granbom, Umberto Martini, Agnieszka Morillon, Roland Pietruck, and Sara Rosendahl. Reuse and recycling of by-products in the steel sector: Recent achievements paving the way to circular economy and industrial symbiosis in europe. *Metals*, 10(3):345, Mar 2020.

[3] Opus International Consultants Ltd. Use of melter slag as aggregate in open-graded emulsion mixes. Technical Report 112, Transfund New Zealand Research Report, 1998.

[4] Domitille Le Cornec, Laurence Galoisy, Laurent Izoret, Laurent Cormier, Nicolas Trcera, and Georges Calas. Structural role of titanium on slag properties. *Journal of the American Ceramic Society*, 2020.

[5] Jan Wiencke, Hervé Lavelaine, Pierre-Jean Panteix, Carine Petitjean, and Christophe Rapin. Electrolysis of iron in a molten oxide electrolyte. *Journal of Applied Electrochemistry*, 48(1):115–126, Jan 2018.

[6] Dihua Wang, Andrew J. Gmitter, and Donald R. Sadoway. Production of oxygen gas and liquid metal by electrochemical decomposition of molten iron oxide. *Journal of the Electrochemical Society*, 158(6):E51–E54, 2011.

[7] A.E. Martin and G. Derge. The electrical conductivity of molten blast-furnace slags. *Trans. Amer. Inst. Min. Met. Eng*, 154:104–115, 1943.

[8] Antoine Allanore. Features and challenges of molten oxide electrolytes for metal extraction. *Journal of The Electrochemical Society*, 162(1):E13–E22, 2015.

[9] Jing Li, Zuotai Zhang, Mei Zhang, Min Guo, and Xidong Wang. The influence of SiO_2 on the extraction of Ti element from Ti-bearing blast furnace slag. *Steel Research International*, 82(6):607–614, 2011.

[10] A. Allanore, L. Yin, and D. R. Sadoway. A new anode material for oxygen evolution in molten oxide electrolysis. *Nature*, 497(7449):353–356, 2013.

[11] Samuel Martin-Treceno, Nicholas Weaver, Antoine Allanore, Catherine M. Bishop, Aaron T. Marshall, and Matthew J. Watson. Electrochemical behaviour of titanium-bearing slag relevant for molten oxide electrolysis. *Electrochimica Acta*, 354:136619, 2020.

[12] Samuel Martin-Treceno, Antoine Allanore, M Bishop, Aaron T Marshall, and Matthew J Watson. Implications of the direct use of slag from ironmaking processes as a molten oxide electrolyte. *JOM*, Accepted:22, March 2021.

[13] Yafei Wang, Jianbang Ge, Weiqian Zhuo, Shaoqiang Guo, and Jinsuo Zhang. Electrochemical extraction of lanthanum in molten fluoride salts assisted by KF or NaF. *Electrochemistry Communications*, 104:106468, 2019.

[14] S. Martin-Treceno, C. Bishop, A. Marshall, and M.J. Watson. Value extraction from waste in the steelmaking industry. In *Chemeca 2018*, pages 28.1–28.9, Queenstown, NZ, 2018. Institution of Chemical Engineers.

[15] Handong Jiao, Donghua Tian, Shuai Wang, Jun Zhu, and Shuqiang Jiao. Direct preparation of titanium alloys from Ti-bearing blast furnace slag. *Journal of The Electrochemical Society*, 164(7):D511–D516, 2017.

[16] Handong Jiao, Donghua Tian, Jiguo Tu, and Shuqiang Jiao. Production of $Ti - Fe$ alloys via molten oxide electrolysis at a liquid iron cathode. *RSC Adv.*, 8:17575–17581, 2018.

[17] C.W. Bale, E. Belisle, P. Chartrand, S.A. Decterov, G. Eriksson, A.E. Gheribi, K. Hack, I.-H. Jung, Y.-B. Kang, J. Melancon, A.D. Pelton, S. Petersen, C. Robelin, J. Sangster, P. Spencer, and M.-A. Van Ende. Factsage thermochemical software and databases, 2010 - 2016. *Calphad*, 54:35 – 53, 2016.

[18] Handong Jiao, Qiuyu Wang, Jianbang Ge, Haobo Sun, and Shuqiang Jiao. Electrochemical synthesis of Ti_5Si_3 in $CaCl_2$ melt. *Journal of Alloys and Compounds*, 582:146 – 150, 2014.

[19] G. Frommeyer and R. Rosenkranz. Structures and properties of the refractory silicides Ti_5Si_3 and $TiSi_2$ and Ti-Si-(Al) eutectic alloys. In Oleg N. Senkov, Daniel B. Miracle, and Sergey A. Firstov, editors, *Metallic Materials with High Structural Efficiency*, pages 287–308, Dordrecht, 2004. Springer Netherlands.

[20] E. A. Gulbransen, K. F. Andrew, and F. A. Brassart. Oxidation of molybdenum 550°C to 1700°C. *Journal of The Electrochemical Society*, 110(9):952–959, 1963.

[21] J. E. Campbell, H. B. Goodwin, H. J. Wagner, R. W. Douglass, and B. C. Allen. Introduction to metals for elevated-temperature use. Technical report, Defense Metals Information Center, Battelle Memorial Institute, Ohio, 1961.

[22] Yunming Gao, Chuanghuang Yang, Canlei Zhang, Qingwei Qin, and George Z. Chen. Magnesia-stabilised zirconia solid electrolyte assisted electrochemical investigation of iron ions in a $SiO_2 - CaO - MgO - Al_2O_3$ molten slag at 1723 K. *Phys. Chem. Chem. Phys.*, 19:15876–15890, 2017.

[23] J. Van Der Colf and D. D. Howat. Rates of oxygen removal from titaniferous oxide melts in graphite crucibles. *Journal of The South African Institute of Mining and Metallurgy*, 79(12):343–347, 1979.

[24] Gabriella Tranell, Oleg Ostrovski, and Sharif Jahanshahi. The equilibrium partitioning of titanium between Ti^{3+} and Ti^{4+} valency states in CaO-SiO_2-TiO_x slags. *Metallurgical and Materials Transactions B*, 33(1):61–67, 2002.

[25] Ivan P Ratchev and Geoff R Belton. A study of the liquidus temperatures of titano-magnetite smelting type slags. In *5th International Conference on Molten Slags, Fluxes and Salts*, pages 387–393, 1997.

[26] D. Sobha Jayakrishnan. 5 - electrodeposition: the versatile technique for nanomaterials. In Viswanathan S. Saji and Ronald Cook, editors, *Corrosion Protection and Control Using Nanomaterials*, Woodhead Publishing Series in Metals and Surface Engineering, pages 86 – 125. Woodhead Publishing, 2012.

[27] T.B. Massalski, J.L. Murray, L.H. Bennett, and H. Baker. *Binary Alloy Phase Diagrams*. American Society for Metals, 1990.

[28] Yulai Song, Zhihe Dou, Ting an Zhang, and Yan Liu. Research progress on the extractive metallurgy of titanium and its alloys. *Mineral Processing and Extractive Metallurgy Review*, 0(0):1–17, 2020.

[29] Yun Lei, Chao Wang, Wenhui Ma, Jijun Wu, Kuixian Wei, Shaoyuan Li, Guoqiang Lv, and Kazuki Morita. A novel approach to prepare high-purity Si and $Si/TiSi_2$ materials simultaneously using Ti-bearing blast furnace slag. *Journal of Alloys and Compounds*, 798:333 – 341, 2019.

[30] Mansoor Barati and Kenneth S. Coley. Electrical and electronic conductivity of CaO-SiO2-FeOx slags at various oxygen potentials: Part II. Mechanism and a model of electronic conduction. *Metallurgical and Materials Transactions B*, 37(1):51–60, February 2006.

[31] Aida Abbasalizadeh, Annelies Malfliet, Seshadri Seetharaman, Jilt Sietsma, and Yongxiang Yang. Electrochemical extraction of rare earth metals in molten fluorides: Conversion of rare earth oxides into rare earth fluorides using fluoride additives. *Journal of Sustainable Metallurgy*, 3(3):627–637, 2017.

[32] L. Zhang and J. Wu. Ti_5Si_3 and Ti_5Si_3-based alloys: Alloying behavior, microstructure and mechanical property evaluation. *Acta Materialia*, 46(10):3535–3546, 1998.

[33] R. Rosenkranz, G. Frommeyer, and W. Smarsly. Microstructures and properties of high melting point intermetallic Ti_5Si_3 and $TiSi_2$ compounds. In S.H. WHANG, D.P. POPE, and C.T. LIU, editors, *High Temperature Aluminides and Intermetallics*, pages 288 – 294. Elsevier, Oxford, 1992.

[34] Thomas Hughes. The development of ultra-high temperature experimental capabilities for the electrolytic extraction of titanium from New Zealand Steel's iron slag. Thesis, University of Canterbury, 2018.

[35] S. Prasad and A. Paul. Growth mechanism of phases by interdiffusion and atomic mechanism of diffusion in the molybdenum-silicon system. *Intermetallics*, 19(8):1191–1200, 2011.

Figure captions

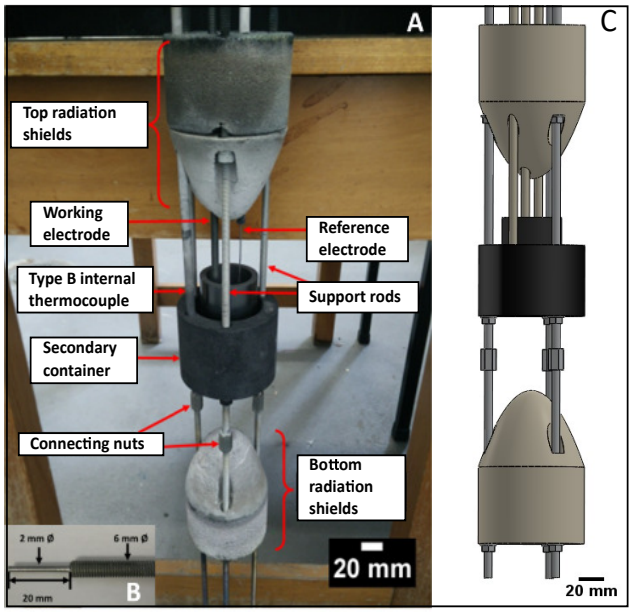

Figure 1. Electrochemical cell used in the vertical tube furnace adapted from [34], showing (A) the various individual components of the internal support structure system and (B) the modified area of the molybdenum working electrode in contact with the slag. (C) is the computer-aided design drawing of the set-up.

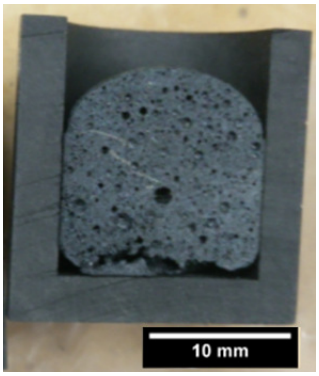

Figure 2. Slag A after being fired to operating temperatures in a graphite crucible. The convex meniscus indicates a lack of reactive wetting.

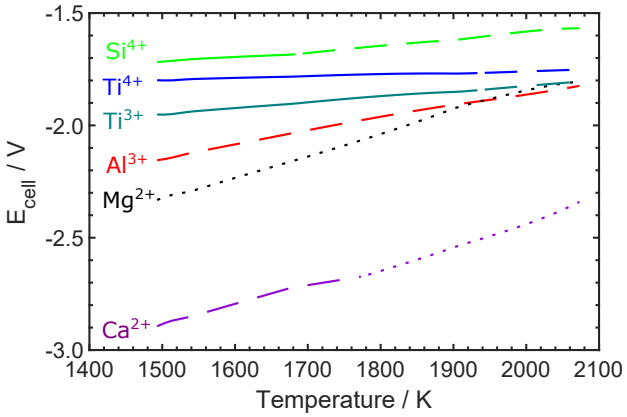

Figure 3. Thermodynamic cell voltage sequence for Slag A. Cell reactions are reduction of molten metal oxide to a pure metallic phase with O_2 evolution. The line type represents the state of the stable metallic phase formed at the specified temperature: solid (solid line), liquid (dashed line) and gas (dotted line).

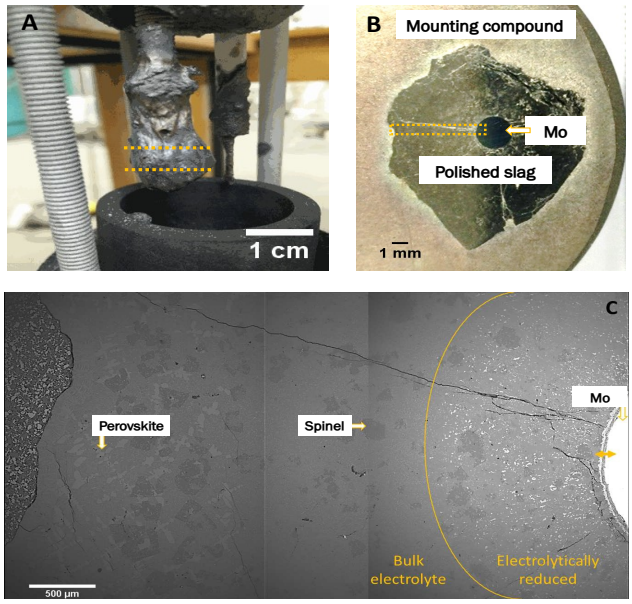

Figure 4. Procedure for the microscopy analysis after potentiostatic electrolysis of Slag A. (A) portion of the WE pulled out of the molten slag after electrolysis. (B) polished cross-section of the electrode, indicated by orange line in previous image, embedded in mounting compound. (C) composite of three back-scatter electron images of the area surrounding the Mo WE, orange rectangle in (B), containing the bulk slag and the region containing electrolytically reduced products. EDS analysis for orange arrow at WE surface is presented in Figure 5.

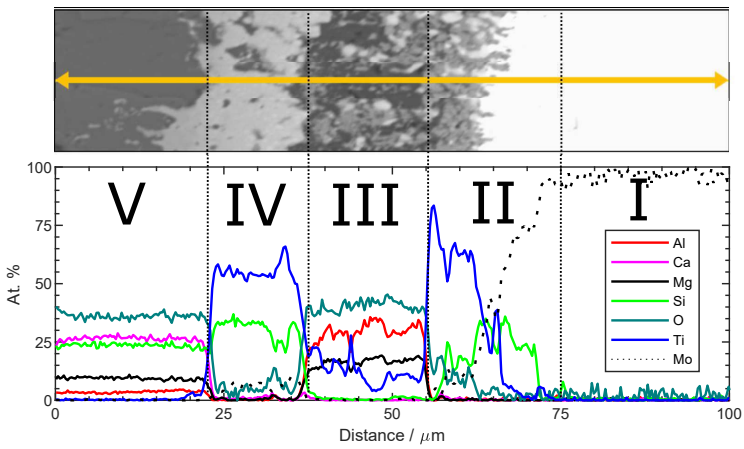

Figure 5. EDS linescan of the reduced layer around the molybdenum working electrode indicated by orange arrow in Figure 4C for Slag A. Region I corresponds to the core of the Mo WE, Regions II and IV are part of the products of the electrolysis, and Regions III and V are phases representative of the bulk electrolyte.

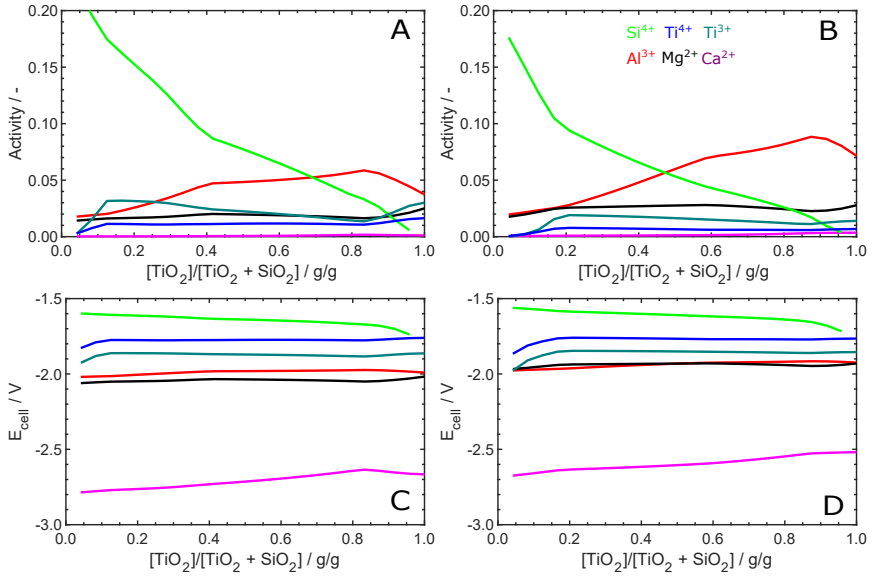

Figure 6. Effect of changing the fraction of TiO_2, with a fixed total SiO_2 + TiO_2 in the slag, on the predicted thermodynamic activities referenced to pure oxides in the slag phase (A and B), and the cell voltages for the reduction of metals and evolution of O_2 gas (C and D) for 1773 K and 1873 K, respectively.

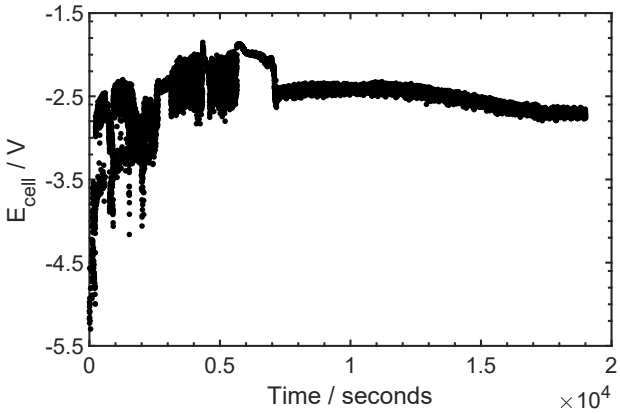

Figure 7. Cell voltage vs time plot recorded from a galvanostatic electrolysis experiment for Slag B. Current held at 5 A ($(10.0 \pm 3.8)\,\mathrm{A\,cm^{-2}}$) for 317 min at 1823 K.

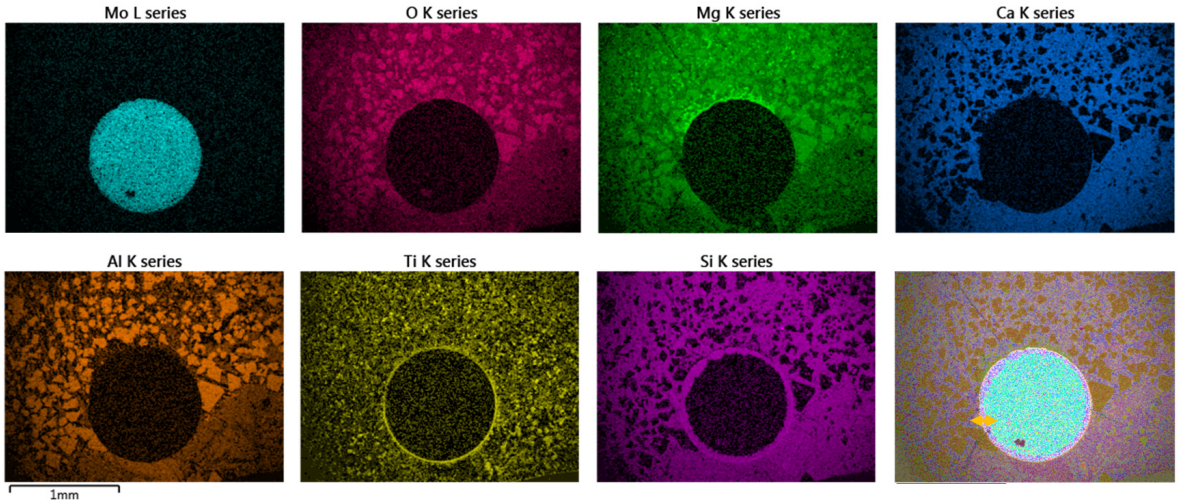

Figure 8. EDS composition maps of the molybdenum working electrode and the electrolytic deposit surrounding it after the galvanostatic experiment performed on Slag B, showing the same product morphology as Slag A in Figure 5.

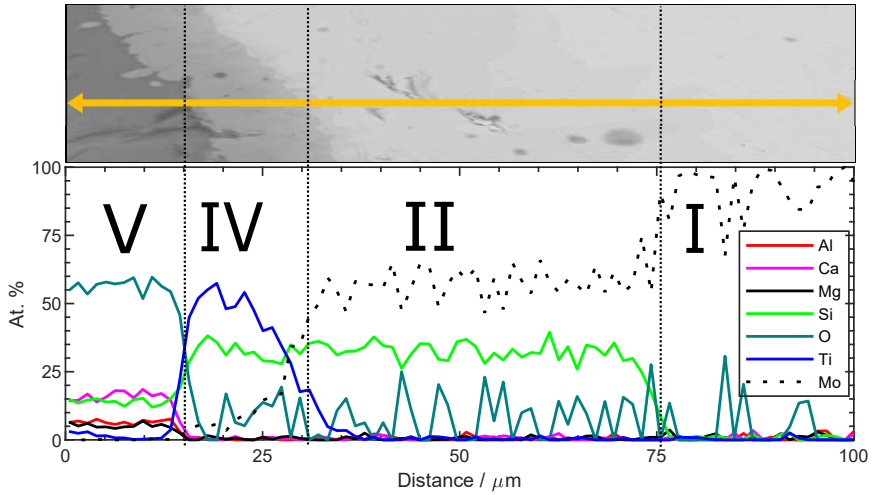

Figure 9. EDS linescan of the various product regions formed in the reduced layer around the molybdenum working electrode shown in Figure 8.

Tables and table captions

Table 1. Electrolyte compositions (wt%) measured by XRF.

	TiO_2	CaO	SiO_2	Al_2O_3	MgO
Slag A	33	18	15	19	15
Slag B	9	25	26	20	19

Table 2. Gibbs energy of formation for binary Si-Ti-Mo intermetallics in descending order predicted for the stable phases at 1823 K [27,35] using FactSage's FTlite database.

			$\Delta G^{\circ}_{formation}$ (kJ mol^{-1})
Si (l) + 3Mo (s)	$\longleftrightarrow$	Mo_3Si (s)	-118
Si (l) + Ti (s)	$\longleftrightarrow$	TiSi (s)	-131
2Si (l) + Mo (s)	$\longleftrightarrow$	$MoSi_2$ (s)	-147
3Si (l) + 5Mo (s)	$\longleftrightarrow$	Mo_5Si_3 (s)	-339
3Si (l) + 5Ti (s)	$\longleftrightarrow$	Ti_5Si_3 (s)	-564
4Si (l) + 5Ti (s)	$\longleftrightarrow$	Ti_5Si_4 (s)	-634